Available online at www.sciencedirect.com
SCIENCE DIRECT®
International Journal of Heat and Mass Transfer 47 (2004) 4659–4672
International Journal of HEAT and MASS TRANSFER
www.elsevier.com/locate/ijhmt

Laminar convective heat transfer from a circular cylinder exposed to a low frequency zero-mean velocity oscillating flow

Hiroshi Iwai [a,*], Tomoyuki Mambo [a], Naoki Yamamoto [a], Kenjiro Suzuki [b]

[a] Department of Mechanical Engineering, Kyoto University, Yoshida Hon-machi, Sakyo-ku, Kyoto 606-8501, Japan
[b] Department of Machinery and Control Systems, Shibaura Institute of Technology, 307 Fukasaku, Saitama 337-8570, Japan

Received 17 July 2003
Available online 8 June 2004

Abstract

Heat transfer characteristics of a circular cylinder exposed to a slowly oscillating flow with zero-mean velocity were investigated. The flow oscillation amplitude and frequency were changed in the range where the flow remains laminar and fluid particle travels back and forth over much larger distance compared to the cylinder diameter. The time- and space-averaged Nusselt number was measured by transient method, while two-dimensional numerical simulation was conducted to discuss the instantaneous flow and thermal fields around the cylinder. It was found that the time- and space-averaged Nusselt number can be correlated with the oscillating Reynolds number and Richardson number. Unique heat transfer characteristics under oscillating flow condition can be seen at the phases when the cross-sectional mean velocity is small or increasing from small value. During such period, heat transfer can be enhanced due to the local fluid motion induced by the vortices around the cylinder, which once moved away but returned back by the reversed flow. This heat transfer enhancement, however, is countered by the local warming effect of the hot vortices clinging around the cylinder at such phases.

Keywords: Heat transfer; Oscillating flow; Circular cylinder; Low frequency

1. Introduction

Study of flow and heat transfer characteristics of an object mounted in an oscillating flow or of an object reciprocally moving back and forth in a steady flow is important in relation with many practical applications. Large scale examples of them are off-shore structures or long bridges and high towers in stormy conditions, and much smaller ones are flow rate sensors to be mounted in air manifold of auto-engines. Mid-size examples are heat regenerators for Stirling engines and cryocoolers. Flow and heat transfer characteristics of these examples, not only the instantaneous ones but also the time averaged ones, should be different from the counterparts of steady flow condition and are actually affected by the frequency and amplitude of oscillating flow as well as the time-mean flow Reynolds number. All the related phenomena should be quasi-steady when flow velocity changes slowly with small amplitude. In the cases of zero-mean velocity oscillating flows, however, flow around an obstacle reverses its direction form one half cycle to another and a peculiar effect may appear in relation with this flow reversal. Velocity and thermal wakes and vortices moved away in a direction in a precedent half cycle of flow oscillation return back to the obstacle in the following half cycle by the flow reversal. This may affect the flow and heat transfer characteristics

* Corresponding author. Tel.: +81-75-753-5218; fax: +81-75-753-5203.
E-mail address: iwai@mech.kyoto-u.ac.jp (H. Iwai).

0017-9310/$ - see front matter © 2004 Elsevier Ltd. All rights reserved.
doi:10.1016/j.ijheatmasstransfer.2003.08.031

Nomenclature

A	amplitude of fluid particle displacement, m
A_s	surface area of cylinder per unit length, m^2
c	heat capacity of cylinder material, J/kg K
D	cylinder diameter, m
f	frequency of flow oscillation, Hz
g	acceleration of gravity, m/s^2
Gr_D	Grashof number, $\beta g D^3(T_m - T_a)/\nu^2$
h	heat transfer coefficient, $W/(m^2 K)$
H	height of the test section and computational domain, m
KC	Keulegan–Carpenter number, U_{max}/fD
L	length of the test section and computational domain, m
N	grid number
Nu	Nusselt number, hD/λ_f
Pr	Prandtl number of fluid
Re_{os}	oscillating flow Reynolds number, $U_{eff}D/\nu$
Ri	Richardson number, Gr_D/Re_{os}^2
t	time, s
Δt	averaging time interval, s
T	temperature, K
T_a	initial fluid temperature, K
T_f	film temperature, $(T_{init} + T_a)/2$, K
T_{init}	initial temperature of cylinder, K
T_m	mean temperature of cylinder over the measuring period, K
T_s	surface temperature of cylinder, K
T_w	temperature of channel wall, K
U_{eff}	effective mean velocity of oscillating flow, $2U_{max}/\pi$, m/s
U_{max}	oscillating flow maximum velocity, $2\pi fA$, m/s
W	width of the test section, m

Greek symbols

β	volume expansion ratio of the fluid, 1/K
λ_c	thermal conductivity of cylinder material, W/(m K)
λ_f	thermal conductivity of fluid, W/(m K)
μ	fluid viscosity, Pa s
ν	kinematic viscosity of fluid, m^2/s
ω	oscillation angular frequency, $2\pi f$, rad/s
ρ	fluid density, kg/m^3
Γ	time period of flow oscillation, $1/f$, s

of the obstacle and its effect can be more serious when the frequency of the flow oscillation is low. The present study is an extension of the previous papers treating similar phenomena [1–3] and in particular aims at clarifying how this returning back of the released vortices to the obstacle affects its heat transfer characteristics.

Various research works have been carried out with aims to study general flow characteristics around an object mounted in an oscillating flow. Sarpkaya [4] investigated the fluid force acting on a cylinder and a sphere mounted in an oscillating flow. Williamson [5] studied the flow structure around circular cylinders by making use of a flow visualization technique of dispersing aluminium powder in water, the working fluid. Tatsuno and Bearman [6] also carried out flow visualization using two methods; the electrolytic precipitation method and the aluminium dust method in air flow. In their results, they identified eight regimes of the flow patterns and found the longitudinal flow structures called "streaked flow" and "tubes" appearing intermittently around the object. Ishiwata and Ohashi [7] have investigated the fluid force acting on a cylinder in an oscillating flow condition, while Okajima et al. [8] have carried out flow visualization for both of circular and square cylinders. Classification of flow structures has been made in the latter study. Concerning numerical simulations, two-dimensional laminar flow computations of a uniform stream passing an oscillating cylinder have been carried out using the finite difference method by Hurlbut et al. [9]. Development of turbulence models and study of turbulence structures for the oscillating flow around a circular cylinder have been carried out by several researchers including the Refs. [10,11].

In the application of heat regenerators, heat transfer characteristics of an elementary object composing of the heat transfer matrix in the zero-mean velocity oscillating flow conditions are particularly important. Related to the flow structures studied so far, it is expected that heat transfer characteristics of an elementary object in oscillating flow condition should be different from that immersed in a steady flow, but have rarely been studied so far. Heat transfer studies for a similar geometry can also be found in high frequency or thermo-acoustic field condition, but oscillating flows in such conditions are very much different from what is expected in the case of a regenerator.

Hamaguchi et al. [12] conducted experimental works on the pressure loss and heat transfer characteristics of the stack of wire mesh gauzes in a one-direction steady and unsteady flow field. Tanaka et al. [13] carried out an experimental study on the fluid flow and heat transfer characteristics of several wire-mesh stack of different specification placed in an oscillating flow. The basic idea of this type of investigations is to provide a database for the heat transfer and pressure drop characteristics of a heat exchanger matrix. The provided databases are

useful in a practical design to assess its performance of the regenerator having the studied matrix. However, for optimizing the size and geometry of a regenerator matrix to be used under a given operation condition, more detailed studies have to be made.

The present authors recently measured a time- and space-averaged Nusselt number of a circular cylinder mounted in a zero-mean velocity oscillating flow by making use of a transient method, with which cooling process of a heated cylinder has been measured. They presented a relationship correlating the averaged Nusselt number with the oscillating flow Reynolds number and the Grashof number [1]. However in that work, cylinder diameter was fixed at one size and the Grashof number remained almost the same value for all the studied cases. The presented relationship, therefore, need to be revisited with new experimental data to be obtained with a cylinder of different size. Furthermore, the information obtained with the transient method is limited to a time- and space-averaged value. More detailed information such as spatial distribution of Nusselt number, its time history etc. cannot be obtained with such procedure. Numerical simulation is expected to be an effective approach to have such information. This study focuses on a circular cylinder placed in a sinusoidally oscillating flow, which is an elementary object to form the wire mesh matrix of the regenerator. Therefore, in this article, characteristics of the convective heat transfer from a circular cylinder placed in an oscillating flow are discussed based on the results both of experiment and numerical simulation.

2. Experimental apparatus and procedure

2.1. Experimental set-up

Because the details of the experimental procedure can be found in Iwai et al. [1], only its basic feature is explained here. As is seen in Fig. 1, an oscillating air flow is generated in the test section by driving a piston in a piston-cylinder assembly back and forth to breeze in and out air from an open end of the test section. Its frequency f is changed by adjusting the rotational speed of the piston-driving motor. As was described in the Ref. [1], the stroke of the piston A_p can be adjusted independently from f. The actual values of f and A_p were measured with a laser displacement sensor and the inaccuracy of their values was judged to be 1% and 3%, respectively. The amplitude of fluid particle displacement, A, is calculated with the value of A_p taking account of the cross-sectional area ratio between the piston assembly and test section. The values of A and f will be used in the following as parameters to specify the velocity amplitude $U_{max}(=2\pi fA)$ in place of U_{max} itself. A fibre-scope sensor was installed in a piston assembly to generate electronic pulse signal as the reference for specifying the phase of the flow oscillation. The test section is 600 mm long and has a 150×150 mm square cross section. Honeycombs are placed at both ends of the test section to calm the approaching flow turbulence.

Fig. 2 shows the layout of the test section. The origin of the coordinate system is located at the center of the test section where the heated circular cylinder is introduced at the start of the experiment through the sidewall. Two test cylinders having different diameter, D, are used; previously used diameter 10 mm and newly used one in the present study 8 mm. The blockage ratio for each case is $D/H = 0.067$ and 0.053, respectively. This value is sufficiently small compared to Okajima et al. [8] and Kikuchi et al. [14] and small enough to neglect the channel wall effect. Difference of diameter is only 20% between the two cylinders but the smaller to larger case ratio of Grashof number is 1/2 because Grashof number is proportional to D^3. Therefore this difference of cylinder diameter is just sufficient to discuss the effect of Grashof number on the time- and space-averaged Nusselt number. Cylinder to fluid initial temperature

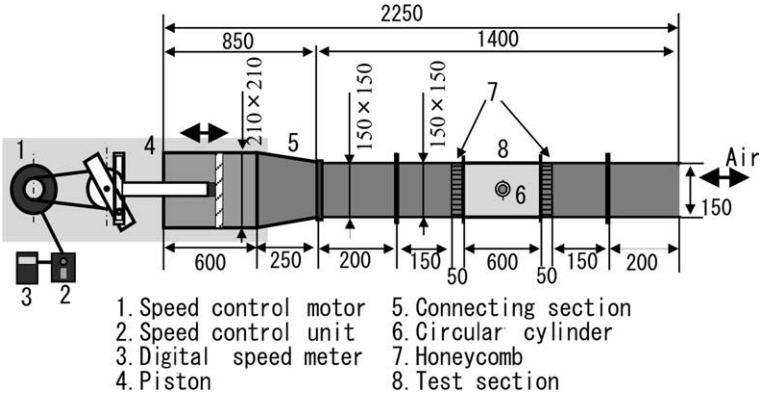

Fig. 1. Experimental apparatus.

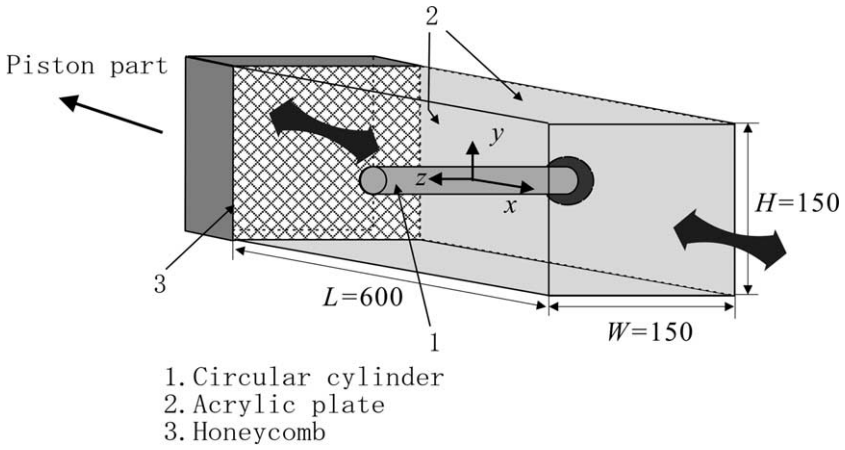

Fig. 2. Test section.

difference was about 80 K and the corresponding value of the Grashof number was in the range $3000 < Gr_D < 3300$ in the present experiment for $D = 8$ mm.

The experimental conditions adopted in the present experiment were $0.2 \leqslant f \leqslant 1.1$ Hz and $10 \leqslant A/D \leqslant 38$. This corresponds to the range of the oscillating flow Reynolds number $40 < Re_{os} < 810$, which is defined as $Re_{os} = U_{eff}D/v$. Here the velocity scale U_{eff} is the mean absolute bulk velocity of the oscillating flow averaged over one oscillating cycle, $U_{eff} = (2/\pi)U_{max} = 4fA$. The Keulegan–Carpenter number, KC, defined as $KC = U_{max}/fD$ ranges in the present study as $63 < KC < 240$. The presently studied condition is therefore the case where low frequency oscillating flow remains laminar [15,16] and fluid particle travels back and forth over much larger distance compared to the cylinder diameter. In other words, the time period of flow oscillation is of the length within which more than several pairs of vortices would be formed if velocity is kept constant at the value U_{max}.

2.2. Smoke flow visualization

The smoke flow visualization experiment was conducted to visualize the flow field around the circular cylinder. For this purpose, the smoke of incense sticks was introduced into the test section as the tracer for visualization and the sheet beam of Argon-ion laser was applied to illuminate the smoked flow pattern image in vertical and horizontal mid planes of the test section. A home video camera and a digital still camera were used as the recording devices.

2.3. Heat transfer measurement and data reduction

A primary difficulty of heat transfer measurement in an oscillating flow condition arises from the fact that the same fluid moves back and forth inside the test section. Employing a normal steady-state heat transfer measurement, fluid inside the test section is continuously heated by the heat transferred from the cylinder, resulting in an increase of the fluid temperature around the cylinder. This makes the definition of heat transfer coefficient unclear and also results in an unavoidable error in heat transfer measurement.

To cope with this problem, time- and space- averaged (overall) Nusselt number is measured by transient method [17] in this study. Test cylinder shown in Fig. 3 is made of copper. Its large thermal conductivity was effective to secure the uniformity of temperature inside the cylinder at any stage of the whole cooling process with good accuracy. E-type thermocouples inserted from both side ends of the cylinder were used to measure the cylinder temperature. Acrylic pipes attached to both ends of the cylinder were effective to reduce the heat loss from the mid part of the cylinder toward its ends. The cylinder is first heated outside, then quickly inserted into the test section and exposed to the oscillating flow. The recorded time history of the cylinder temperature was used to obtain the time- and space-averaged Nusselt number.

Ignoring the heat loss from the both ends of the cylinder, heat balance equation for the cylinder becomes two dimensional. Further neglecting the radiative heat transfer from the cylinder surface, it yields

$$Mc\frac{dT}{dt} + hA_s(T - T_a) = 0, \quad (1)$$

where M and A_s are respectively the mass and the surface area of the cylinder per its unit length and c its specific heat, h is the space-averaged heat transfer coefficient over the cylinder surface, T and T_a are the instantaneous cylinder and initial fluid temperatures, respectively. Biot number is smaller than 10^{-3} in the case of this experi-

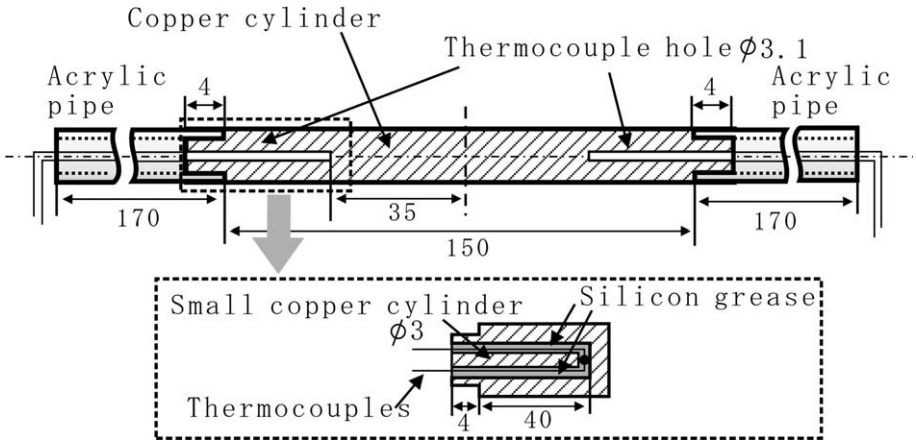

Fig. 3. Copper cylinder for heat transfer measurement.

ment so that the temperature uniformity inside the cylinder is actually attained with good accuracy. Two time dependent quantities T and h are now decomposed into their time-averaged components $\langle T\rangle$ and $\langle h\rangle$ and their fluctuating components T' and h'. Averaging time interval $\Delta t = (t - t_{\text{init}})$, which is equal to the measuring time interval, can be taken to be much larger compared with the period of flow oscillation, if the cooling process proceeds slowly enough. Then, the time average of a fluctuating quantity can be set equal to zero. Thus, the time-averaged form of Eq. (1) becomes

$$Mc\frac{\mathrm{d}\langle T\rangle}{\mathrm{d}t} + \langle h\rangle A_{\mathrm{s}}(\langle T\rangle - T_{\mathrm{a}}) = 0. \tag{2}$$

Assuming that $\langle h\rangle$ is independent of the temperature level, Eq. (2) is integrated as

$$\ln\left[\frac{\langle T\rangle - T_{\mathrm{a}}}{T_{\mathrm{init}} - T_{\mathrm{a}}}\right] = -\frac{\langle h\rangle A_{\mathrm{s}}}{Mc}(t - t_{\mathrm{init}}), \tag{3}$$

where T_{init} is the initial cylinder temperature at $t = t_{\mathrm{init}}$. If plotted on a semi-logarithmic diagram, this relationship should result in a straight line. In cases where the obtained relationship is not linear, the proposed procedure is not applicable. Fig. 4 shows a typical example of the time history of the measured cylinder temperature. The linear relationship expressed in Eq. (3) obviously holds during the cooling process and applicability of the transient method to the present problem is now confirmed. Considering the results of preliminary sensitivity tests, data reduction for $\langle h\rangle$ was decided to be done over the first fifty cycles or the averaging time interval, Δt, was fixed at 50 times the period of flow oscillation in all the studied conditions. The overall time- and space-averaged Nusselt $\overline{Nu}$ number is then defined using the value of $\langle h\rangle$ as

$$\overline{Nu} = \frac{\langle h\rangle D}{\lambda_{\mathrm{f}}}. \tag{4}$$

All the properties of the fluid and the cylinder material were evaluated at the initial film temperature, $T_{\mathrm{f}} = (T_{\mathrm{init}} + T_{\mathrm{a}})/2$.

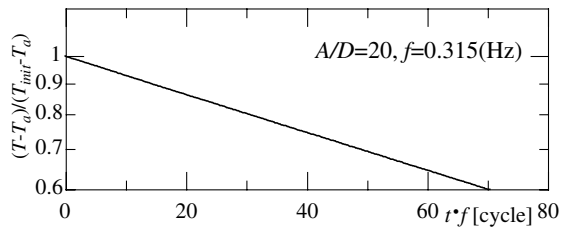

Fig. 4. Typical time history of test cylinder temperature.

3. Numerical procedure

The above mentioned experimental approach is effective to measure the overall heat transfer characteristics of the cylinder. However, it is not enough to obtain detailed information needed in the comprehensive analysis of the phenomenon. Therefore, numerical simulations are combined in this study for this purpose. Computation has been carried out with a computational model developed to suit this purpose under the conditions set as close to the experimental counterparts as possible. However to save the computer resources and computational time, several assumptions were employed in the numerical simulation. Two-dimensional numerical simulation is conducted for the flow and thermal fields in a computational domain of a channel having the streamwise length L schematically illustrated in Fig. 5. Cylinder of the diameter $D = 10$ mm is located at the center of the domain and the channel height was taken to be $H/D = 15$ while streamwise length of the computational domain was set $L/D = 30$. Spatial periodicity

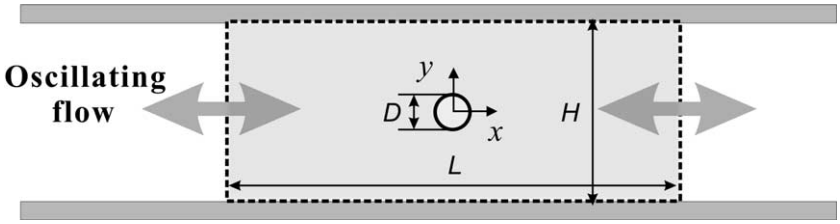

Fig. 5. Computational domain.

was applied at the upstream and downstream boundaries of the computational domain. Composite grid system developed by Xi et al. [18] was applied. In this method, two types of grid systems are allocated in the computational domain. One is the Cartesian main co-ordinate grid system and the other is the cylindrical sub co-ordinate grid one. The main one covers the entire computational domain while the sub grid system is used only near the circular cylinder as schematically shown in Fig. 6. The origins of the both co-ordinate systems are placed at the center of the cylinder.

The working fluid is air and its properties are assumed constant. Buoyancy effect is neglected in the computation. Thus, for the Cartesian co-ordinate system, the governing equations may be the following forms of the time-dependent, two-dimensional incompressible continuity, Navier–Stokes and energy equations

$$\left(\frac{\partial u_j}{\partial x_j}\right) = 0, \tag{5}$$

$$\frac{\mathrm{D}\rho u_i}{\mathrm{D}t} = -\frac{\partial p}{\partial x_i} + \frac{\partial}{\partial x_j}\left(\mu\frac{\partial u_i}{\partial x_j}\right), \tag{6}$$

$$\frac{\mathrm{D}\rho T}{\mathrm{D}t} = \frac{\partial}{\partial x_j}\left(\frac{\mu}{Pr}\frac{\partial T}{\partial x_j}\right). \tag{7}$$

Here $\mathrm{D}/\mathrm{D}t = \partial/\partial t + u_i(\partial/\partial x_i)$ where $i, j = 1, 2$. Spatial periodicity assumed in x-direction for the velocity components, u and v, and temperature, T, is described as follows:

$$\phi(x, y) = \phi(x + L, y), \tag{8}$$

where ϕ represents u, v or T. Hence the boundary conditions can alternatively be expressed as

$$\phi(x_{\mathrm{right}}, y) = \phi(x_{\mathrm{left}}, y), \tag{9}$$

where x_{right} and x_{left} mean the positions of the right and left ends of the computational domain. Relationship must be modified for the pressure p since the pressure drop occurs in the x-direction. To consider the pressure drop in the streamwise direction, Navier–Stokes equations are modified following the Refs. [19,20]. A fully developed periodic flow assumed in those studies are now expanded and it is now assumed that a fully developed periodic flow situation holds at every instant during the oscillation. The local pressure is decomposed into a linear part and a periodic fluctuation part as follows:

$$p(x, y) = -\alpha x + P(x, y), \tag{10}$$

where αx represents the linear pressure drop. Substituting this into the Navier–Stokes equations, they can be remodeled as

$$\frac{\partial u}{\partial t} + u\frac{\partial u}{\partial x} + v\frac{\partial u}{\partial y} = -\frac{1}{\rho}\frac{\partial P}{\partial x} + \nu\left(\frac{\partial^2 u}{\partial x^2} + \frac{\partial^2 u}{\partial y^2}\right) + \alpha, \tag{11}$$

$$\frac{\partial v}{\partial t} + u\frac{\partial v}{\partial x} + v\frac{\partial v}{\partial y} = -\frac{1}{\rho}\frac{\partial P}{\partial y} + \nu\left(\frac{\partial^2 v}{\partial x^2} + \frac{\partial^2 v}{\partial y^2}\right), \tag{12}$$

where α is the pressure gradient to generate the corresponding mass flow in the channel. To establish an oscillating flow it is set

$$\alpha = A\omega^2 \cos\omega t. \tag{13}$$

Then the boundary condition for pressure becomes

$$P(x_{\mathrm{right}}, y) = P(x_{\mathrm{left}}, y). \tag{14}$$

All the governing equations shown above are for the Cartesian co-ordinate system. For cylindrical co-ordinate system, equations have been transformed appropriately.

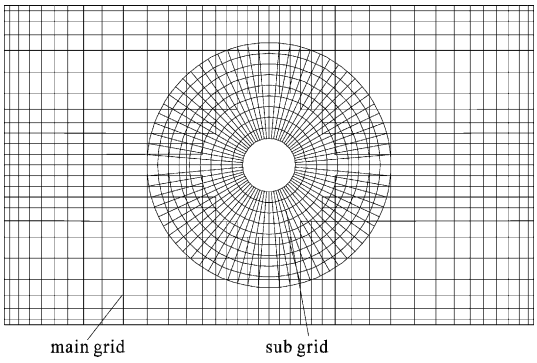

Fig. 6. Image of composite grid system.

Governing equations are discretized by finite volume method. The program code is developed based on the code developed by Onishi et al. [21]. QUICK and central difference schemes are applied for convection and diffusion terms respectively. SIMPLE algorithm is used for the computation of pressure correction in the iteration procedure. The time increment between two successive time steps is set so that the Courant number for the smallest grid spacing is equal to unity. At every time step, a maximum of 25 iterations are applied in the solution procedure of the equations.

Staggered grid system is employed in both the Cartesian and cylindrical co-ordinate grid systems. Grid points are allocated non-uniformly in the computational domain, finely near the solid surfaces where large gradients of velocity and temperature are expected to appear. Prior to the parameter study, the effects of the grid system and of the number of the allocated grid points have been checked and consequently $(N_x, N_y) = (382, 304)$ grid points for the main grid system and $(N_r, N_\theta) = (30, 81)$ grid points for the sub grid system have been chosen.

The circular cylinder is maintained at a constant uniform temperature, T_s, while the channel wall surface temperature is also kept constant and uniform at T_w slightly lower than T_s. Therefore the working fluid is heated by the cylinder and cooled at the two channel wall surfaces. No slip condition is used on the solid surfaces. In streamwise direction, as mentioned above, spatially periodical boundary condition is applied to reduce the computational load.

Computations have been carried out for four cases shown in Table 1. Namely, the oscillating amplitude is varied in two steps of $A/D = 10$ and 20 while its frequency is also changed in two steps at $f = 0.6$ and 1.0 Hz. The cylinder diameter is set at $D = 10$ mm. Obtained results are compared with the experimental counterpart of each condition. Close attention is paid to the flow and thermal fields around the cylinder, the local Nusselt number distribution on the cylinder surface as well as its time history. The local Nusselt number is calculated from the numerical results as

$$Nu = \frac{q_s D}{\lambda_f (T_s - T_w)},$$

where q_s is the local heat flux on the cylinder surface.

Table 1
Computational conditions

Case no.	A/D	f [Hz]
1	10	0.6
2	10	1
3	20	0.6
4	20	1

4. Heat transfer measurement and numerical model assessments

4.1. Oscillating flow profile

Prior to the heat transfer measurement, the oscillating flow field without the insertion of a circular cylinder was examined. Time change of the fluid velocity was found to almost follow a sinusoidal curve only showing a slight deviation when the reverse flow velocity takes its peak. No prominent high frequency components of velocity change was observed showing that the studied flow is laminar. It was also confirmed that the boundary layers along the channel walls were not so developed and the cross-stream distribution of velocity in a channel was very close to that of a uniform flow. On the whole, it was confirmed that a sinusoidal oscillating laminar flow with uniform cross-sectional velocity profile was established when no cylinder was inserted. Details can be found in Iwai et al. [1].

4.2. Heat transfer measurement

To confirm the propriety of the transient method adopted in this study for determining the time- and space-averaged heat transfer coefficients, preliminary experiments were conducted using the test cylinder in a static environment. The obtained experimental results were found to agree well with the experimental relationship for the natural convection around a horizontal cylinder [22] as is described in the Ref. [1]. This confirms the capability of the transient method as a heat transfer measurement technique.

4.3. Oscillating flow in simulation

To validate the present computational scheme of calculating the oscillating flow by making use of the spatial periodicity assumption, a test calculation was conducted for a two-dimensional fully-developed channel flow without an insertion of a cylinder. Theoretical streamwise velocity profile can be analytically obtained for this flow as reported by Ohmi et al. [23]. Fig. 7

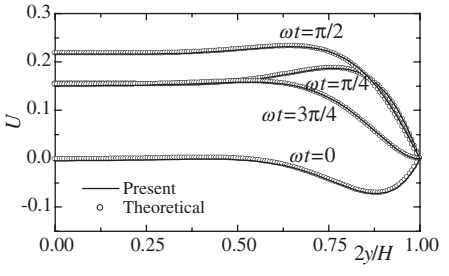

Fig. 7. Velocity profiles for fully developed oscillating flow.

compares the present numerical results of the velocity profiles at four different phases of the flow oscillation with the theoretical counterparts. Because of the symmetric nature of the flow, profiles are illustrated only in a half of the channel in this figure. As clearly observed in the figure, the present numerical results show an excellent agreement with the theoretical velocity profiles. This validates the present numerical scheme of treating the oscillating flow.

4.4. Numerically obtained overall Nusselt number

Overall Nusselt number $\overline{Nu}$ is shown in Fig. 8 for the calculated four cases in comparison with their experimental counterparts. There are four major assumptions adopted in the numerical computation, namely the two-dimensionality and the spatial periodicity of the flow and thermal fields, artificial cooling of the fluid at the channel wall and the elimination of the buoyancy effect. Effects of the first two have been confirmed to be small in the preliminary computation. As seen in the figure, the obtained results stay fairly close to the experimental data so that the effectiveness of the present computation is confirmed. The numerical results of $\overline{Nu}$ are slightly lower than the experimental data. One possible reason for this is the buoyancy effects ignored in the numerical computation. First, free-forced combined convection is formed around the cylinder due to the buoyancy effects as in the steady flow case reported by Collis and Williams [24] for thin heated wires. In the second, buoyancy deflects the streamlines of reversed flow of hot wake up away the cylinder. The first one is effective to raise the value of $\overline{Nu}$ and the second one is effective to reduce the suppression effect of heat transfer to be discussed later. Especially, the second effect is characteristic only to the oscillating flow and can occur in any oscillating flow condition at the phases where flow velocity is small.

Although the present numerical computation does not precisely agree with the experiments, its results are judged to be available in analyzing the basic features of the flow and thermal fields around the circular cylinder mounted in an oscillating flow with zero-mean velocity.

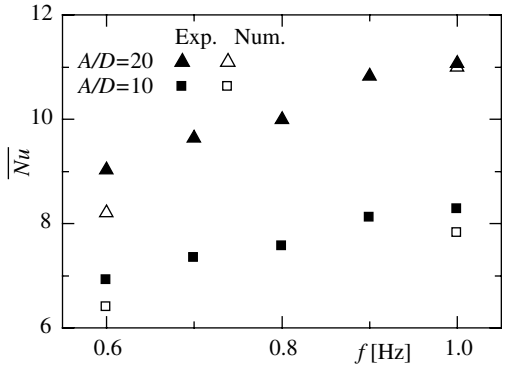

Fig. 8. Comparison of overall Nusselt number with experimental data.

5. Results and discussion

5.1. Flow around a circular cylinder in an oscillating flow

Fig. 9 shows the photographs of the illuminated flow pattern around the circular cylinder taken through the transparent side walls for a case of $A/D = 10$ and $f = 0.2$ Hz. The pictures were taken at the four consecutive phases astride the zero-crossing time of velocity and apart from each other by an interval $\Gamma/15$, where $\Gamma = 1/f$ is the time period of flow oscillation. The white horizontal arrow attached to each photograph indicates the direction and magnitude of the instantaneous cross-sectional mean velocity. Fig. 9(a) shows the vortices generated on the right side back of the cylinder by the rightward flow. As the flow is reversed toward the left, the vortices generated in the previous half cycle and once moved away to the right come back to the cylinder and cover its surfaces as shown in Fig. 9(b). This flow reversal and return of the released vortices back to the cylinder are the unique features of the present flow. It is observed in Fig. 9(d) that the two vortices can still be identified although they are moving away to the left conveyed by an increased flow velocity. Fig. 9(e) shows the photograph showing the flow pattern in a horizontal plane slightly above the cylinder position. This is taken at an instant when the flow began to reverse to the left side of this figure or in between the instants of Fig. 9(a) and (b). Although the existence of some three dimensional structure is seen in the right end region of the photograph, almost two dimensional rolling up of smoked sheet is observed on the right side of the cylinder within the distance of 2–3 times the cylinder diameter. This suggests that two-dimensionality characterizes the flow around the cylinder at least in the middle part of the cylinder. This is consistent with the fact that the cylinder aspect ratio, W/D, does not affect the measured overall Nusselt number.

5.2. Overall Nusselt number

Here is first discussed the overall Nusselt number, the time- and space-mean Nusselt number $\overline{Nu}$ obtained in the present study in comparison with the previous results for the case with larger cylinder diameter [1] and, as is described in Chapter 2, the Grashof number is different between the present and previous studies by a factor 2.

The measured value of $\overline{Nu}$ is shown in Fig. 10 for different values of the frequency f of flow oscillation and fluid particle travel distance A. Uncertainty of the pres-

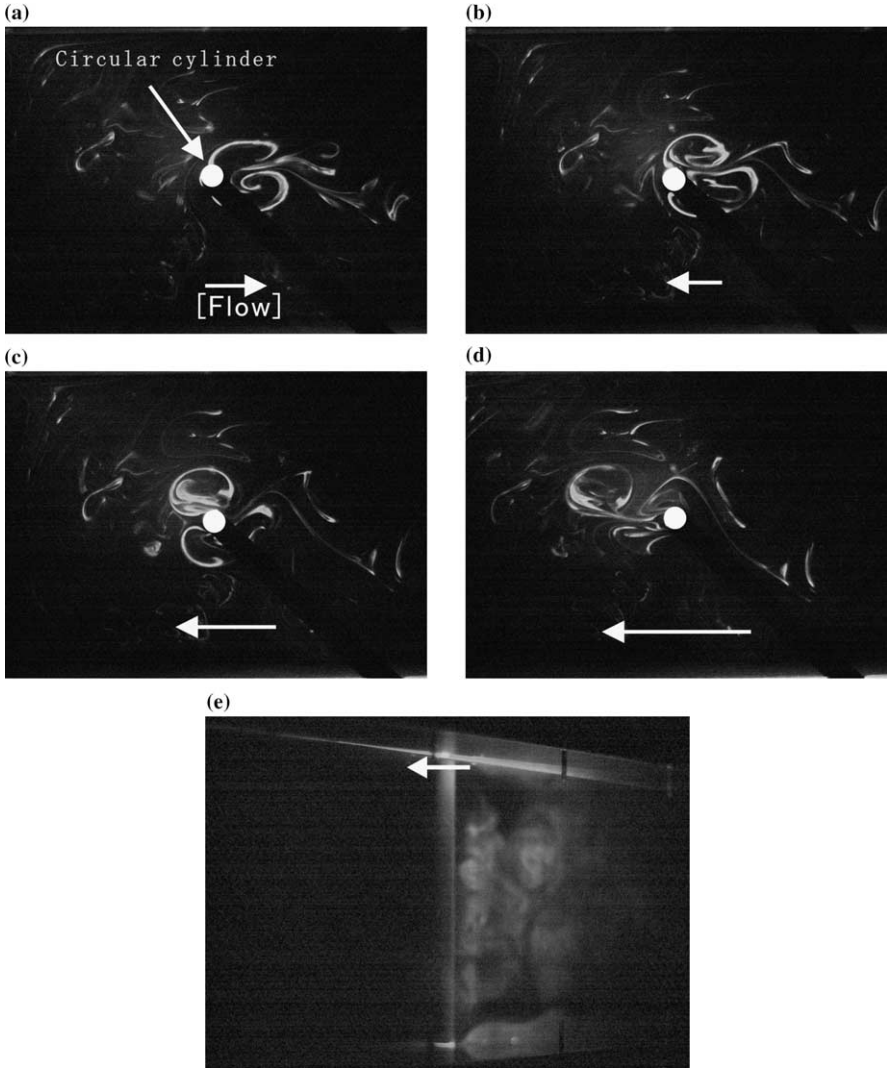

Fig. 9. Flow visualization around the cylinder.

ent heat transfer experiments is estimated to be less than 7%. It is seen in Fig. 10 that in all the studied conditions, the value of $\overline{Nu}$ increases with an increase of f or A. As the value of A increases, $\overline{Nu}$ increases more prominently at higher oscillating frequency. The effect of fluid particle travel distance A seems to be larger at higher oscillating frequency. These characteristics are common for both cases of different cylinder diameter. In Fig. 10(a), it is observed that the $\overline{Nu} - f$ relationship is not perfectly linear but curves with a similar trend for all the cases of different value of A [1].

Logarithmic plot of $\overline{Nu}$ against the oscillating flow Reynolds number, Re_{os} is shown in Fig. 11. Relationship recommended by McAdams [25] for steady flow heat transfer from a circular cylinder can be expressed as $Nu = 0.615Re^{0.466}$ in the range of $40 < Re < 4000$. The broken line in Fig. 11 corresponds to this McAdams equation. Solid squares are for the case of cylinder diameter $D = 10$ mm and blank circles are for the case $D = 8$ mm. Present experimental data almost fall in one straight line in the range of $Re_{os} > 110$ and lie close to the McAdams equation even though the flow structures are totally different between the oscillating flow and steady flow cases as already has been noticed in the results of the flow visualization. Small deviation of the present data from the McAdams equation is not very important, since it can be reduced if a multiplier to U_{eff} is introduced. Such deviation can also result from the above discussed second buoyancy effect. Deviation between the present results and the McAdams equation becomes larger in the lower Reynolds number region, $Re_{os} < 110$. This should be caused by the first buoyancy

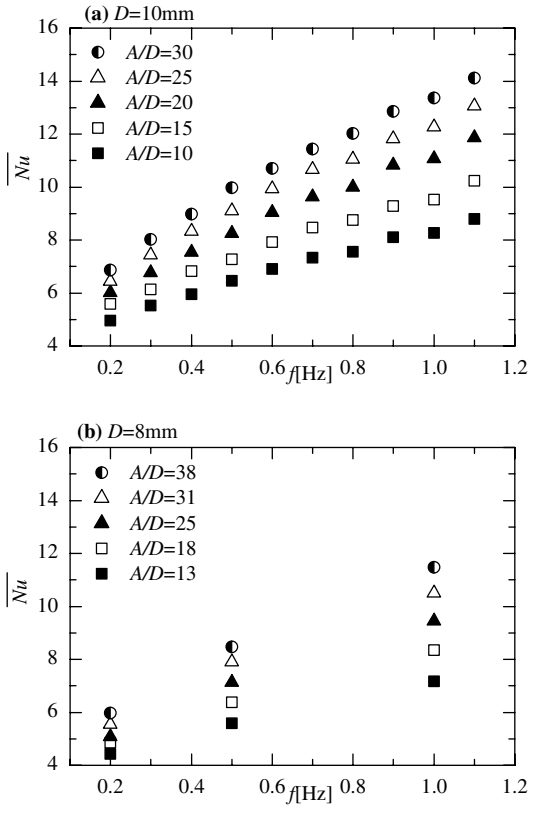

Fig. 10. Effect of oscillating amplitude and frequency on the overall Nusselt number.

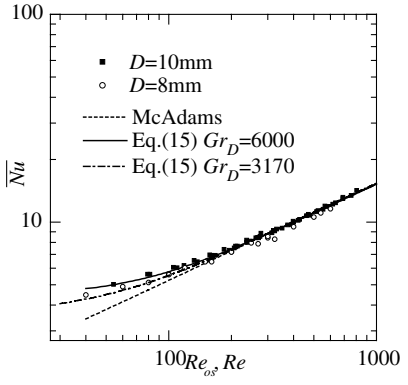

Fig. 11. Re_{os} dependency of overall Nusselt number.

effect or the generation of free-forced combined convection as discussed in the Ref. [1]. Less noticeable deviation of the present experiments from the McAdams equation reflects the fact that the Grashof number is smaller with smaller size cylinder. The previously proposed relationship in the Ref. [1] for this Reynolds number range was:

$$Nu = 0.615 Re_{os}^{0.466}(1 + Ri)^{0.2}, \tag{15}$$

where Ri is the Richardson number, defined as $Ri = Gr_D/Re_{os}^2$ and $Gr_D = \beta g D^3(T_m - T_a)/v^2$. T_m is the time mean temperature of the cylinder over the measuring period of time of heat transfer. The coefficient 0.615 and the exponent 0.466 were taken from the McAdams equation and the exponent for Ri was chosen to have the best fit to the previous experimental data obtained with the cylinder of $D = 10$ mm. Two lines plotted in the figure represent Eq. (15) respectively for the two cases of $Gr_D = 6000$ and $Gr_D = 3170$. They agree fairly well respectively with the previous and present experimental data indicating the applicability of Eq. (15) to the cases of different Grashof number.

5.3. Details of the flow and thermal fields

Now the numerical results are presented here to discuss the basic heat transfer characteristics and the details of the flow and thermal fields around the cylinder. First, Fig. 12 gives the time history of the space-averaged Nusselt number, Nu_{sp}, for one oscillating period of time for a case of $A/D = 10$ and $f = 1.0$ Hz. The hollow circles are included for the reference in this figure to show the quasi-steady value of Nu_{sp} to be obtained by applying the McAdams equation for the velocity at each phase of flow oscillation. The changing pattern of numerically obtained value of Nu_{sp} is close to its quasi-steady counterpart and Nu_{sp} is largest around the phases $\omega t = \pi/2$ and $3\pi/2$ when the absolute value of the instantaneous bulk velocity is largest. These indicate that the instantaneous thermal boundary layer formed around the cylinder surface at those phases would be similar to that in steady flow condition. Noticeable difference between an oscillating flow case and a steady flow case is observed at the decelerating phases of flow velocity $3\pi/4 < \omega t < \pi$ and $7\pi/4 < \omega t < 2\pi$. Conspicuous sharp drop of Nu_{sp} appears particularly around the phases $\omega t = 2\pi/5$ and

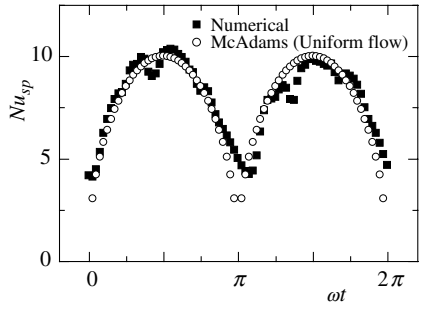

Fig. 12. Time history of space averaged Nusselt number.

$\omega t = 4\pi/3$. This is the effect of the hot wake and vortices once moved-away from the cylinder but coming back to and clinging for a while around the cylinder. This will be discussed more in detail later.

Fig. 13 shows the distribution of the time-averaged local Nusselt number, $\overline{Nu_\theta}$, on the cylinder surface. Peripheral angle θ is measured anti-clockwise from the x-axis. Since the buoyant force is ignored in the numerical computation, time-averaged velocity and thermal fields around the cylinder should be symmetric with respect to x-axis as well as to y-axis. Asymmetry of the distribution of $\overline{Nu_\theta}$ resulted from insufficient length of averaging time. Its background will be discussed later and is left unimproved as it is seen in the figure since the illustrated results are enough just for the discussion to follow. It is seen in Fig. 13 that comparing four cases presently calculated for the same cylinder diameter, $D = 10$ mm, $\overline{Nu_\theta}$ becomes larger at any position with an increase of Re_{os} which is proportional to fAD. Difference is small between the two cases of $A/D = 20$, $f = 0.6$ and of $A/D = 10$, $f = 1.0$ since Re_{os} is different only 20% between the two cases. $\overline{Nu_\theta}$ takes highest value $\overline{Nu}_{\theta,\max}$ at $\theta = 0$ and π, and the lowest $\overline{Nu}_{\theta,\min}$ at $\theta = \pi/2$ and $3\pi/2$ in all the four cases. The ratio $\overline{Nu}_{\theta,\max}/\overline{Nu}_{\theta,\min}$ becomes larger for higher Re_{os} case. Its value is 1.7 when $A/D = 20$ and $f = 1.0$ or $Re_{os} = 545$, while it is 1.4 when $A/D = 10$ and $f = 0.6$ or $Re_{os} = 163$.

Fig. 14 shows the instantaneous vorticity contour maps near the cylinder sampled at several phases in the range $\pi/2 \leqslant \omega t \leqslant 11\pi/8$ for a case of $A/D = 10$, $f = 1$ as an example. In the first half of the cycle $\pi/2 \leqslant \omega t \leqslant \pi$, flow is decelerating and cross-sectional mean velocity becomes zero at $\omega t = \pi$. In the second half of the cycle

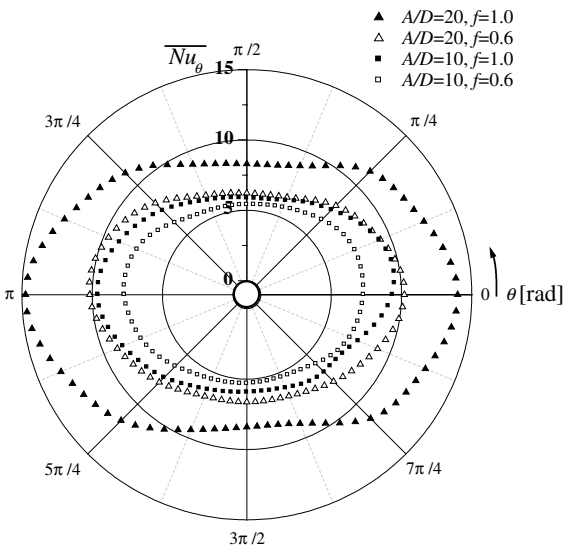

Fig. 13. Time averaged local Nusselt number.

$\pi \leqslant \omega t \leqslant 11\pi/8$, flow is accelerating but in the reversed direction. Note that only the region around the cylinder, that is $-5 \leqslant x/D \leqslant 5$ and $-5 \leqslant y/D \leqslant 5$, is shown in these figures. Shaded parts correspond to the area of positive vorticity and white parts to the negative. Formation of Kármán vortices is clearly observed at the decelerating phases at the downstream side, or at the right side, of the cylinder. Vortices are also formed at the accelerating phases but not in such a clear pattern as observed at the decelerating phases. In the final period of decelerating phase and in the beginning of the accelerating phase, velocity becomes small. Therefore, the formation of vortices also slowed down. Fig. 14(e) corresponds to an instant when the cross-sectional mean velocity is zero. At this moment, fluid near the cylinder is not quiet yet but moving by viscous effect and by the flow induced by the vortex generated just before but still staying near the cylinder. At the following accelerating phases, some old vortices moved away sometime before to the right return back to and stay around the cylinder. Each of them induces a circulating flow around its respective position. This vortex-inducing flow affects the new formation of vortices and their positions and motions near the cylinder. This results in the asymmetric clinging pattern of new and old vortices around the cylinder at these phases. The asymmetry of local time-mean Nusselt number found in Fig. 13 is related to this instantaneous asymmetry of the flow pattern.

Comparing this figure with Fig. 15, which illustrates the fluid temperature contours around the cylinder at the same instants, it is found that the locations of the vortices well coincide the high fluid temperature regions. This means that the new and old vortices returning back and clinging around the cylinder have not been amply cooled down. Therefore, due to this warming effect, the stirring flow generated around the cylinder as the superposition of the flows induced by every vortices is not fully effective to enhance the heat transfer from the cylinder.

Fig. 16 shows the distribution of the instantaneous local Nusselt number Nu_θ on the cylinder surface sampled at the same phases as those of Figs. 14 and 15. When the cross-sectional mean velocity is high, at the phase $\omega t = \pi/2$ for example, Nu_θ is larger on the side $3\pi/4 < \theta < 5\pi/4$, which is upstream side at this instant, and smaller on the downstream side. This is a feature quite similar to that in a steady flow case [26]. At $\omega t = \pi$ when the cross-sectional mean velocity is zero, Nu_θ takes large value around the peripheral position $\theta = \pi/4$. A pair of counter rotating vortices is observed in Fig. 14(e) around this position. The left one accompanies clockwise rotating fluid motion and the right one anti-clockwise fluid rotation. Therefore, in between the two vortices, flow is induced so as to entrain the cold fluid from the outer region and to feed it toward the cylinder surface. This results in a large temperature gradient at

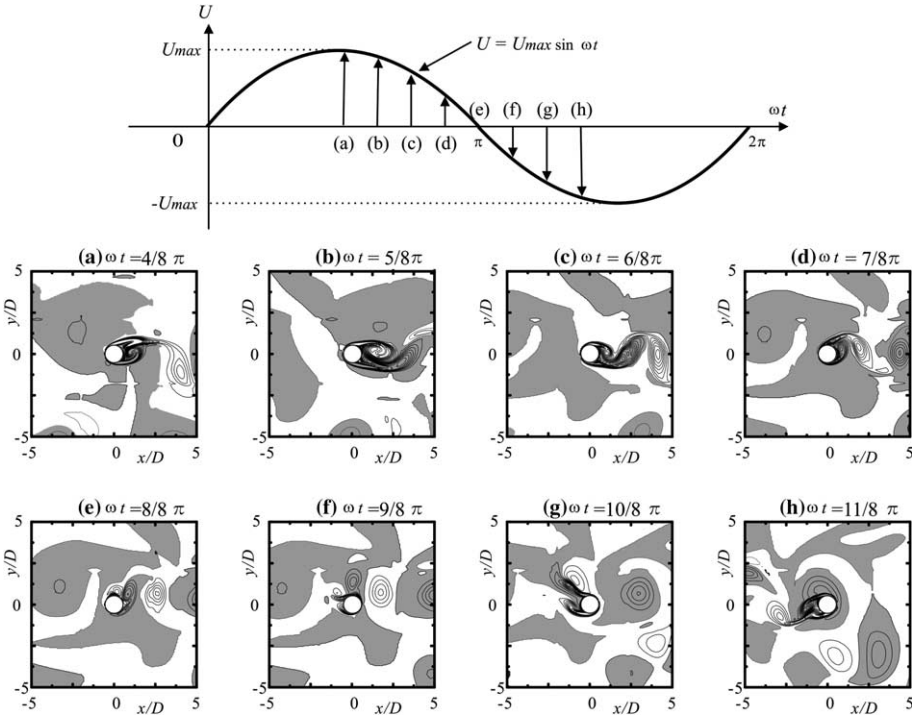

Fig. 14. Time variation of vorticity contours around the cylinder for a half cycle.

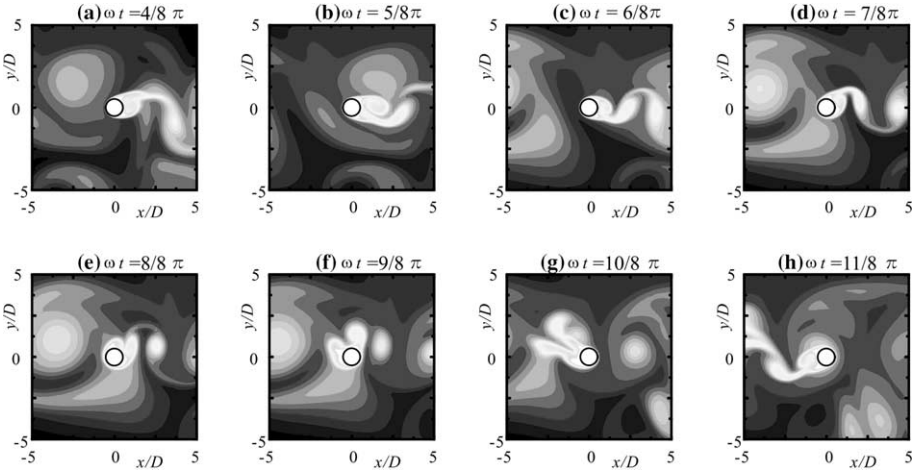

Fig. 15. Time variation of temperature contours around the cylinder for a half cycle.

the cylinder surface there. This is the position around $\theta = \pi/4$. This indicates that, even when the cross-sectional mean velocity is zero or quite small, heat transfer can be enhanced due to the local fluid motion induced by the vortices, once moved away but returned back conveyed by the reversed flow and then staying for a while near the cylinder. This phenomenon is responsible for the larger value of space-mean Nusselt number Nu_{sp} around $\omega t = \pi, 2\pi$ observed in Fig. 12.

The value of Nu_{sp} does not differ so much between the two phases $\omega t = 5\pi/4$ and $\omega t = 11\pi/8$ even though the cross-sectional mean velocity is higher at $\omega t = 11\pi/8$ as is confirmed in Fig. 14. Distribution of instantaneous local Nusselt number Nu_θ is illustrated in Fig. 16(g) and (h) respectively at the two phases. Comparing Fig. 14(g) and (h) with Fig. 15(g) and (h), it is seen that the hot vortex positioned a little away from the cylinder on its right at the phase $\omega t = 5\pi/4$ returns back so as to sur-

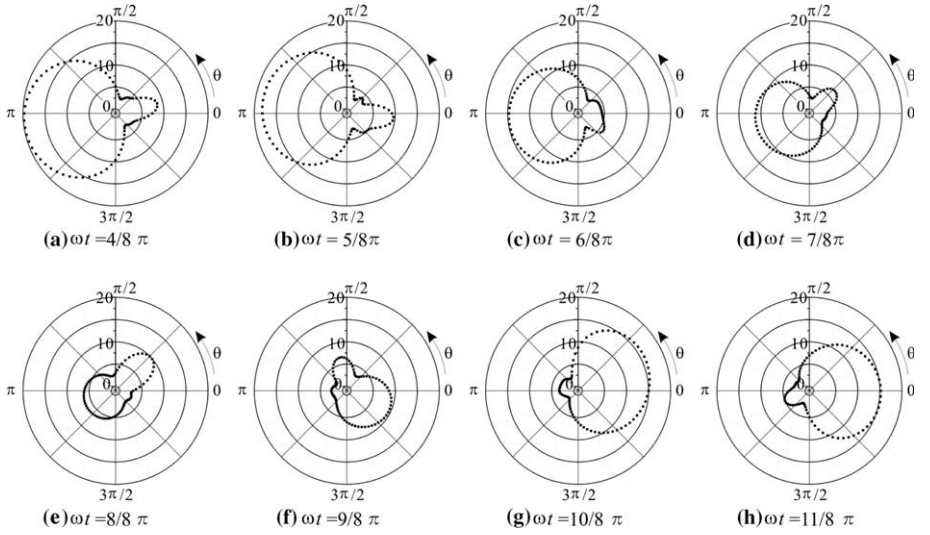

Fig. 16. Time variation of instantaneous local Nusselt number, Nu_θ, distribution.

round the cylinder at the next phase $\omega t = 11\pi/8$. As has been discussed above, the enhancement of heat transfer due to the acceleration of cross-sectional mean flow is affected by the local velocity field generated as the superposition of the velocity field induced by each of the vortices staying around the cylinder. This local velocity field effect is further countered by the local warming effect, i.e. the heat transfer suppression caused by the clinging of the hot old vortices around the cylinder. This is the background why the value of Nu_{sp} at the phase $\omega t = 11\pi/8$ does not differ so much from that at the previous phase $\omega t = 5\pi/4$. Conspicuous drop of Nu_{sp} observed around the phase $\omega t = 4\pi/3$ in Fig. 12 also results from the same phenomenon. Vortices formation and the cross-sectional mean flow variation occur at their own respective periodicity. So the phase difference between the heat transfer enhancement due to the local velocity effect and heat transfer suppression due to the local warming effect varies from one cycle of the cross-sectional mean flow oscillation to another. Therefore the magnitude and phase of the sharp drop of Nu_{sp} fluctuate rather irregularly from one cycle to another of the cross-sectional mean flow oscillation. Harmonic flow oscillation assumed in the analyses [2,3] should only be realized when the cylinders are located at small streamwise pitch.

6. Conclusions

Heat transfer characteristics of a circular cylinder exposed to the slowly oscillating flow with zero-mean velocity were investigated. The flow oscillation amplitude and frequency were changed in the range of $10 \leqslant A/D \leqslant 38$ and $0.2 \leqslant f \leqslant 1.1$ Hz in the experiments. Reynolds number is set small and the flow remained laminar. Flow field was visualized by smoke method and the time- and space-averaged Nusselt number was measured by transient method. Two-dimensional numerical simulation was conducted and discussion was developed for the instantaneous flow and thermal fields around the cylinder. Main conclusions obtained are summarized as follows:

1. Experimentally obtained time- and space-averaged Nusselt number $\overline{Nu}$ can be correlated with the oscillating Reynolds number based on U_{eff}, the effective mean velocity of the oscillating flow, and with the Richardson number (or with the Grashof number) by Eq. (15) within the inaccuracy of 5%.
2. Numerically obtained instantaneous value of space-averaged Nusselt number Nu_{sp} can roughly be approximated with its quasi-steady value. However noticeable discrepancy is found at the phases when the cross-sectional mean velocity is small. Conspicuous sharp drop of Nu_{sp} also occurs in the accelerating flow phase.
3. The thermal boundary layer established on the cylinder surface in the oscillating flow condition is similar to that in steady flow condition in the period of time when the cross-sectional mean oscillating flow velocity is large. When the cross-sectional mean velocity is quite small or when it is increasing from small value, heat transfer can be enhanced due to the local fluid motion induced by the vortices around the cylinder, which once moved away but returned back by the reversed flow. This heat transfer enhancement is

countered by the local warming effect of the hot vortices clinging around the cylinder at such phases.

Acknowledgements

This paper is supported in part by Center of Excellence for Research and Education on Complex Functional Mechanical Systems (COE program of the Ministry of Education, Culture, Sports, Science and Technology, Japan).

References

[1] H. Iwai, T. Mambo, K. Nakabe, K. Suzuki, Time- and space-averaged convective heat transfer from the surface of a circular cylinder in an oscillating flow, in: J. Taine (Ed.), Proceedings of 12th International Heat Transfer Conference, vol. 2, Elsevier, 2002, pp. 777–782.

[2] K. Muralidhar, K. Suzuki, Heat transfer from an array of cylinders in oscillatory flow, in: Proceedings of the 6th ASME-JSME Thermal Engineering Joint Conference CD-ROM, 2003, TED-AJ03-661.

[3] K. Muralidhar, K. Suzuki, Heat transfer from an array of cylinders in oscillatory flow, International Journal of Heat Exchangers, submitted for publication.

[4] T. Sarpkaya, Force on a circular cylinder in viscous oscillatory flow at low keulegan-carpenter numbers, Journal of Fluid Mechanics 165 (1986) 61–71.

[5] C.H.K. Williamson, Sinusoidal flow relative to circular cylinders, Journal of Fluid Mechanics 155 (1985) 141–174.

[6] M. Tatsuno, P.W. Bearman, A visual study of the flow around an oscillating circular cylinder at low Keulegan–Carpenter numbers and low stokes numbers, Journal of Fluid Mechanics 211 (1990) 157–182.

[7] R. Ishiwata, H. Ohashi, Fluid forces on a cylinder in oscillating flow, 1st report, sinusoidal oscillation, Trans. JSME B 50 (449) (1990) 265–273.

[8] A. Okajima, T. Matsumoto, S. Kimura, Force measurements and flow visualization of bluff bodies in oscillatory flow, J. Wind Eng. Indust. Aerodyn. 69–71 (1997) 213–228.

[9] S.E. Hurlbut, M.L. Spaulding, F.M. White, Numerical solution for laminar two dimensional flow about a cylinder oscillating in a uniform stream, Trans. ASME J. Fluids Eng. 104 (1982) 214–222.

[10] M. Kato, B.E. Launder, The modeling of turbulent flow around stationary and vibrating square cylinders, in: Proceedings 9th Symposium on Turbulent Shear Flows, 1993, pp. 10-4-1–10-4-6.

[11] H. Kawamura, N. Kawashima, An application of a near wall k–$\tilde{\varepsilon}$ model to the turbulent channel flow with transpiration and to the oscillatory flow around a square cylinder, in: Proceedings of the 2nd Symposium on Turbulence, Heat and Mass Transfer, 1997.

[12] K. Hamaguchi, S. Takahashi, H. Miyabe, Pressure drop of regenerator matrix, Trans. JSME B 48 (435) (1982) 2207–2216.

[13] M. Tanaka, I. Yamashita, F. Chisaka, Flow and heat transfer characteristics of Stirling engine regenerator in oscillating flow, Trans. JSME B 55 (516) (1989) 2478–2485.

[14] Y. Kikuchi, H. Suzuki, M. Kitagawa, M. Takeuchi, Effect of pulsating Strouhal number on heat transfer around a heated cylinder in pulsating cross-flow, Trans. JSME B 65 (633) (1999) 1724–1730.

[15] M. Ohmi, M. Iguchi, F. Akao, Trans. JSME B 49 (447) (1983) 2343–2353.

[16] P. Merkli, H. Thomann, Transition to turbulence in oscillating pipe flow, J. Fluid Mech. 68 (3) (1975) 567–575.

[17] C.H. Cheng, H.N. Chen, W. Aung, Experimental study of the effect of transverse oscillation on convection heat transfer from a circular cylinder, Trans. ASME J. Heat Transfer 119 (1997) 474–482.

[18] G.N. Xi, K. Torikoshi, K. Kawabata, K. Suzuki, Numerical analysis of unsteady flow and heat transfer around bodies using a compound grid system, Trans. JSME B 61 (585) (1995) 1796–1803.

[19] H. Iwai, H. Watanabe, K. Tatsumi, K. Suzuki, Conjugate heat transfer for a minimal unit model of counter flow type corrugated primary surface heat exchangers, International Journal of Heat Exchangers 4 (1) (2003) 1–26.

[20] S.V. Patankar, C.H. Liu, E.M. Sparrow, Fully developed flow and heat transfer in ducts having streamwise-periodic variations of cross-sectional area, J. Heat Transfer 99 (1977) 180–186.

[21] H. Onishi, K. Inaoka, K. Suzuki, K. Matsubara, Heat transfer performance of a plate-finned tube heat exchanger, A three-dimensional steady numerical analysis for a single row tube, in: J.S. Lee (Ed.), Proceedings of the 11th International Heat Transfer Conference, vol. 6, Taylor and Francis, 1998, pp. 227–232.

[22] T. Fujii, M. Fujii, T. Honda, Theoretical and experimental studies of the free convection around a long horizontal thin wire in air, in: U. Grigull, E. Hahne, K. Stephan, J. Straub (Eds.), Proceedings of the 7th International Heat Transfer Conference, vol. 2, Hemisphere, 1982, pp. 311–316.

[23] M. Ohmi, M. Iguchi, F. Akao, Trans. JSME B 51 (472) (1985) 3867–3874.

[24] D.C. Collis, M.J. Williams, Two-dimensional convection from heated wires at low Reynolds numbers, J. Fluid Mech. 6 (1959) 357–384.

[25] W.H. McAdams, Heat Transmission, third ed., McGraw-Hill, New York, 1954, pp. 252–281.

[26] E.R.G. Eckert, E. Soehngen, Distribution of heat transfer coefficients around circular cylinders in crossflow at reynolds numbers from 20 to 500, Trans. ASME 74 (3) (1952) 343–347.